Absorption spectra of superconducting qubits driven by bichromatic microwave fields

Jiazheng Pan, Hossein Z. Jooya, Guozhu Sun, Yunyi Fan, Peiheng Wu, Dmitry A. Telnov, Shih-I Chu, and Siyuan Han

Phys. Rev. B **96**, 174518 — Published 27 November 2017

DOI: 10.1103/PhysRevB.96.174518

Absorption spectra of superconducting qubits driven by bichromatic microwave fields.

Jiazheng Pan[1,2], Hossein Z. Jooya[3,4 †], Guozhu Sun[1,2,†], Yunyi Fan[1,2], Peiheng Wu[1,2], Dmitry A. Telnov[5], Shih-I Chu[3,6,†], and Siyuan Han[7,†]

[1]Research Institute of Superconductor Electronics, School of Electronic Science and Engineering, Nanjing University, Nanjing 210093, China

[2]Synergetic Innovation Center of Quantum Information and Quantum Physics, University of Science and Technology of China, Hefei, Anhui 230026, China

[3]Department of Chemistry, University of Kansas, Lawrence, Kansas 66045, USA

[4]ITAMP, Harvard-Smithsonian Center for Astrophysics, Cambridge, MA 02138, USA

[5]Department of Physics, St. Petersburg State University, St. Petersburg 199034, Russia

[6]Center for Quantum Science and Engineering, Department of Physics, National Taiwan University, Taipei 10617, Taiwan

[7]Department of Physics and Astronomy, University of Kansas, Lawrence, Kansas 66045, USA

[†]Correspondence and request for materials should be addressed to G.S. (email:gzsun@nju.edu.cn) or H.Z.J. (email: hzjooya@cfa.harvard.edu) or S.I.C. (sichu@ku.edu) or S.H. (email: han@ku.edu).

Abstract

We report experimental observation of two distinct quantum interference patterns in the absorption spectra when a transmon superconducting qubit, is subject to a bichromatic microwave field with same Rabi frequencies. Within the two-mode Floquet formalism with no dissipation processes, we propose a graph-theoretical representation to model the interaction Hamiltonian for each of these observations. This theoretical framework provides a clear visual representation of various underlying physical processes in a systematic way beyond rotating wave approximation. The presented approach is valuable to gain insights into the behavior of multichromatic field driven quantum two-level systems (qTLS), such as two-level atoms and superconducting qubits. Each of the observed interference patterns are represented by appropriate graph products on the proposed colored-weighted graphs. The underlying mechanisms and the characteristic features of the observed fine structures are identified by the transitions between the graph vertices, which represent the doubly dressed states of the system. The good agreement between the numerical simulation and experimental data confirms the validity of the theoretical method. Such multiphoton interference may be used in manipulating the quantum states and/or generate non-classical microwave photons.

Introduction

Superconducting qubits are one of the most promising candidates for the implementation of circuit quantum electrodynamics (QED) platforms. However, the scalability of these systems remains a major obstacle to continued progress [1,2]. The diagonal coupling (longitudinal coupling) of the system with driving fields has proven to have a high potential for scalability [2]. Superconducting qubit architectures that interact with the external field through off-diagonal time-dependent couplings (transverse couplings) have been extensively studied [3-5]. On the contrary, the longitudinal couplings has been investigated mostly within rotating wave approximation (RWA) [6,7]. It has been shown that the consideration of ac Stark level shift and power broadening is significant for quantitative explanation of multiphoton quantum interference phenomena in strongly driven superconducting qubits, when the rotating-wave approximation (RWA) does not work [8].

Due to a wide range of new nonlinear and multiphoton dynamics, there has been growing interest in going beyond monochromatic excitation of two-level systems. Recently, the interaction of a two-level system with two near-resonant fields has been the subject of both theoretical [9-12] and experimental interest [12-15]. Driving the system with two or more frequencies allows the creation of doubly dressed states and opens up a multitude of additional possibilities in the context of quantum simulation and in manipulating the quantum states and generating non-classical microwave photons [16].

The Rabi resonance in bichromatic fields has been observed in optical experiments. For instance, Saiko*et. et al.* [17,18] showed that in the evolution of a spin qubit driven by the bichromatic field, consisting of a transverse microwave (MW) and a longitudinal radio frequency (RF), the accumulation of dynamic phase during the full period of the slow RF field appears as a shift of the Rabi frequency of the qubit in the MW field. Also, Benhelm *et al.* reported a Mølmer–Sørensen-type gate inducing collective spin flips with a bichromatic laser field [19]. In the study of quantum interference between coupled transitions, the dynamical cancellation of spontaneous emission, appears between different channels of transitions among the dressed states of the driven atoms has been pointed out theoretically [20,21]. This has been experimentally demonstrated by an exciton transition of a self-assembled quantum dot exposed to a bichromatic laser field [22,23]. Besides a few experimental investigations on quantum dots [e.g. 22,23], these dynamical effects have not been fully investigated in superconducting quantum circuits.

The commonly used theoretical framework to explain these kind of phenomena is the well-known dressed atom picture. This formalism was developed by Cohen-Tannoudji and Haroche [24] to explain the behavior of atoms exposed to radio-frequency fields described in terms of photons [25]. In fact, the Floquet quasienergy diagram is equivalent to the fully quantized dressed-atom picture in the limit of strong fields [3]. Generalization of the Floquet theory for non-perturbative treatment of infinite-level systems, including both bound and continuum states, was first introduced by Chu and Reinhardt [26].

Dressed superconducting qubits [27,28], have been theoretically studied [29], and experimentally demonstrated [30,31]. The ”dressing” of qubit by the electromagnetic field splits each level into two giving rise to two new qubits with energy difference equal to the Rabi frequency, Ω. The Rabi frequency is proportional to the amplitude of the electromagnetic field and is usually much smaller than the energy difference between the qubit’s states.

In this joint experimental and theoretical work, we reveal the mechanism of a nonlinear dynamical level splitting of superconducting circuits driven by bichromatic microwave field. The external field possesses two equal amplitude components with frequencies scanned from large detuning to resonance frequencies. We focus on the near resonance frequencies where sub-harmonic resonances generate fringe patterns in the transition probability spectra. We demonstrate these results theoretically by generalizing an intuitive graph-theoretical formalism [32] to model the coupling schemes between the two-level quantum system and the bichromatic external field by appropriate graph products on the proposed colored-weighted graphs. The transitions between the product graph vertices, which present the doubly dressed states of the system, will be analyzed to gain insight into the main features of the reported experimental results.

Experimental Setup and Theoretical Approach

The quantized energy levels of superconducting qubits (e.g. artificial atoms) have been experimentally demonstrated with Josephson junction-based superconducting quantum circuits (SQCs) [33-35]. SQCs can, therefore, serve as a testing ground to investigate fundamental atomic-physics phenomena [28,36], like electromagnetically induced transparency (EIT) [37,38], and Autler-Townes (AT) effect [33,39-41]. The latter is an example of electromagnetic dressing of quantum states, and it has been proposed as a basis for fast, high on/off ratio microwave routers for quantum information [42, 43]. Multi-level structures in SQCs, that are tunable and do not entirely rely on the device characteristics of the junctions, can be constructed by mixing a two-level system with an external field [44].

Our device consists of a superconducting transmon qubit coupled to a three-dimensional aluminum cavity as shown in Fig. 1(a). The length, width and depth of the cavity are 15.5 mm, 4.2 mm and 18.6 mm, respectively. The transmon is made via electron beam lithography and double-angle evaporation [45], in which a single Al/AlO_x/Al Josephson junction is capacitively shunted by two Al pads on a high-resistance Si substrate. The schematic of the experimental set-up is shown in Fig. 1(b). The fundamental TE101 mode of the aluminum cavity is $\omega_{cav}/2\pi = 10.678$ GHz. The device is located in an Oxford Triton 400 dilution refrigerator below 10 mK with magnetic shielding. The microwave lines to the cavity are heavily attenuated at each stage of the dilution refrigerator and sent to the cavity through low-pass filters with cutoff frequency of 12 GHz. The output signal from the cavity is passed through cryogenic circulators and a high-electron-mobility transistor (HEMT) amplifier located in the dilution refrigerator and further amplified at room temperature. It is then mixed down and digitized by a data acquisition card.

Three microwave drives are used in the experiment. Qubit control waves (denoted as probe and coupler) are continuous while readout wave (denoted as cavity) is triggered [46]. Cavity, probe and coupler waves are combined by two power splitters at room temperature before being sent to the dilution refrigerator. In a sampling period, the cavity wave is turned on at time $t = 70$ ns for 2100 ns and the data acquisition card starts to record at time $t = 270$ ns. The repetition rate is 10 kHz so the whole sequence is repeated every 100 μs.

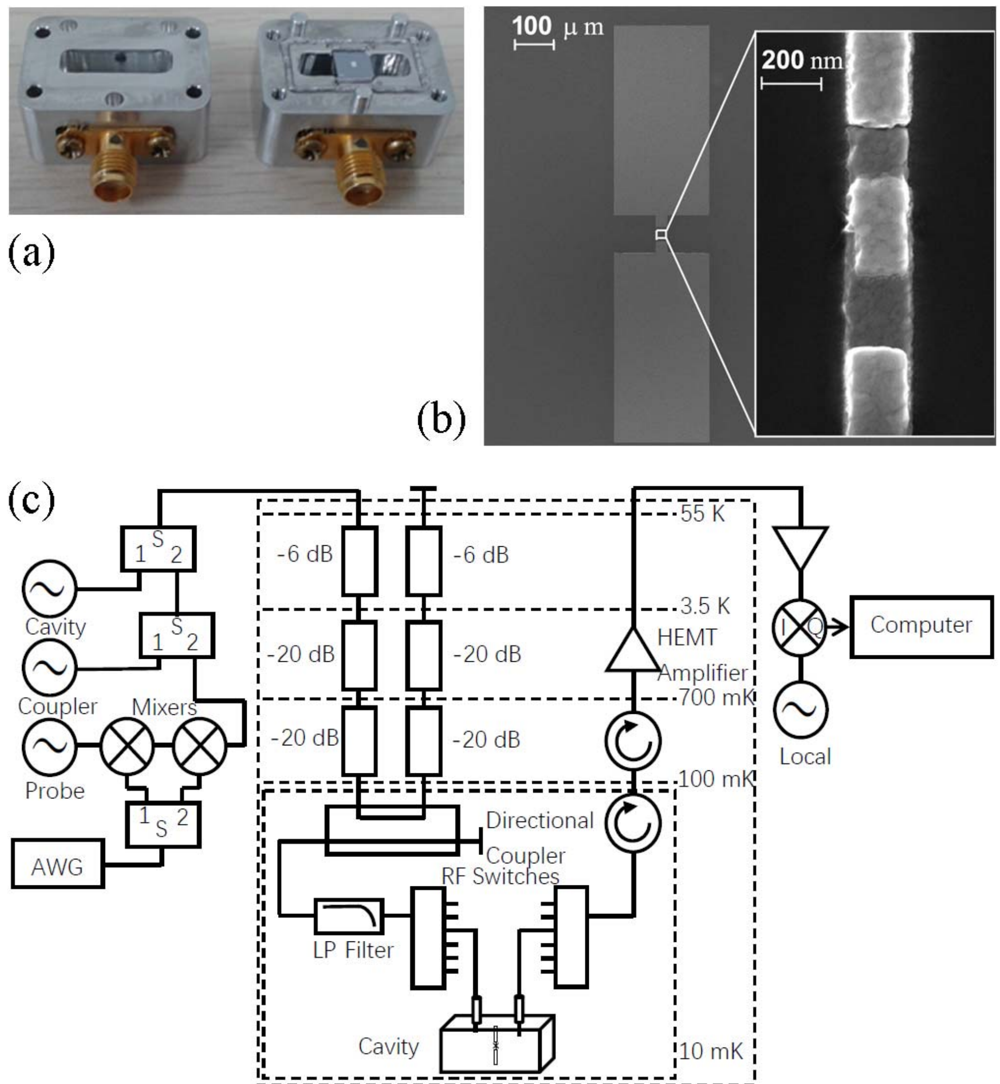

FIG.1. (Color online) (a) An aluminum cavity used to hold the sample. Its fundamental TE101 mode is $\omega_{cav}/2\pi$=10.678 GHz. A transmon qubit on a high-resistance Si substrate is located in the middle of the cavity as shown in the right part of the cavity. (b) Optical (left) and SEM (right) images of a tranmon qubit. A Josephson junction, the middle part shown in the SEM image, is capacitively shunted by two Al pads indicated by the light gray parts in the optical image. (c) Circuit diagram of setup. Attenuators, filters and circulators are used to reduce the external noise. The output signal is then amplified and down-converted with a local oscillator and digitized.

The states of the transmon are measured by using Jaynes-Cummings readout [47]. The cavity wave is applied at the bare cavity frequency $\omega_{cav}/2\pi = 10.678$. We obtain the transition resonance frequency $\omega_{ge}/2\pi = 8.865$ GHz and $\omega_{ef}/2\pi = 8.637$ GHz from the spectrum, from which, we get the Josephson energy $E_J/h = 45.33$ GHz and the charging energy $E_c/h = 228$ MHz. Using pump-probe method we obtain the energy relaxation time $T_1 = 0.53\mu s$. The spin echo measurement shows the dephasing time $T_2 = 0.51\mu s$.

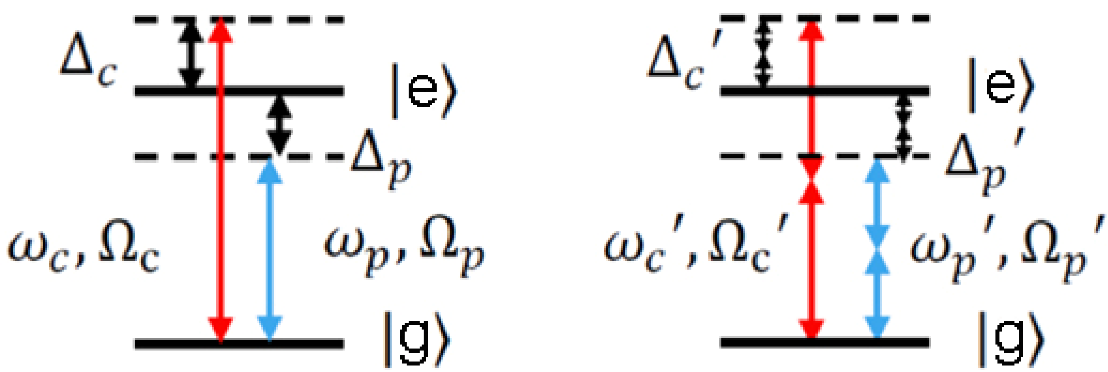

FIG. 2. (Color online) Energy level and microwave drives diagrams represent one-photon transition (left) and two-photon transition (right), respectively.

To demonstrate the effect of two near-resonance driving, probe and coupler waves are turned on continuously, so the system stays at a steady state during the measurement. By sweeping both $\Delta_\mathrm{p} = \omega_p - \omega_{ge}$ and $\Delta_\mathrm{c} = \omega_c - \omega_{ge}$ (which are the detunings of probe and coupler, respectively) around zero, we measure the spectrum of the qubit. As illustrated in Fig. 2, in the one-photon transition experiment, the coupler frequency ω_c and the probe frequency ω_p are both near the transition resonance frequency, ω_ge, and the coupling strengths are $\Omega_c/2\pi = \Omega_p/2\pi = 4.16$ MHz. In the two-photon transition experiment, $\omega_c^{'}$ and ω_p' are near $\omega_{ge}/2$ and $\Omega_c'/2\pi = \Omega_p'/2\pi = 0.973$ MHz.

Natural atoms couple with electromagnetic fields at transverse mode due to the well-defined inversion symmetry of the potential energy. In contrast, transverse and longitudinal couplings between superconducting qubits and classical microwave fields coexist [48]. Within the Bloch representation, the time-dependent Hamiltonian of the system with transverse coupling (without considering the dissipation processes) is given by [5],

$$H_T(t) = -\frac{1}{2}\left[\omega_{ge}\sigma_z + \varepsilon_x(t)\sigma_x\right]. \tag{1}$$

We define $|g\rangle$ and $|e\rangle$ as the eigenstates, and E_g and E_e to be the corresponding eigenvalues of the two-level system. Atomic units, $\mathrm{a.u.}$, are used throughout this paper. We set $\hbar = 1.$ For simplicity, we normalize the parameters by setting the resonance frequency of the system as $\omega_{ge} = 2\pi \times 8.865\ \mathrm{GHz} = 1.0\ \mathrm{a.u}$ during the calculations. The eigenenergy of the bare states of the system are denoted as $E_g = -\frac{1}{2}\omega_{ge}$ and $E_e = \frac{1}{2}\omega_{ge}$. In Eq. (1), $\varepsilon_x(t) = 2b_P cos(\omega_P t + \phi_P) + 2b_C cos(\omega_C t + \phi_C)$ is the bichromatic oscillating interaction connecting (through off-diagonal coupling) the states of the two-level system. ω_P and ω_C are the probe and coupler frequencies, respectively. ϕ_P and ϕ_C are the initial phase of the monochromatic fields. For simplicity we assume $\phi_P = \phi_C = 0$. Therefore, $b_P = V_{ge}^{(P)}$, and $b_C = V_{ge}^{(C)}$. $V_{ge}^{(P)}$ and $V_{ge}^{(C)}$ are the electric dipole moment interactions for the probe and coupler, respectively. For the calculations we use $b_P = b_C = 2.12 \times 10^{-4}\ \mathrm{a.u.}$ σ_x and σ_z are the Pauli matrices. By expanding the total wave function $\psi(t)$ in the basis of $|g\rangle$ and $|e\rangle$, the unperturbed eigenstates of the Hamiltonian becomes [49].

$$i\frac{d}{dt}\begin{pmatrix}\langle g|\psi(t)\rangle\\ \langle e|\psi(t)\rangle\end{pmatrix}=$$

$$\begin{pmatrix}E_g & 2b[\cos(\omega_P t+\phi_P)+Rcos(\omega_C t+\phi_C)]\\ 2b[\cos(\omega_P t+\phi_P)+Rcos(\omega_C t+\phi_C)] & E_e\end{pmatrix}\times$$

$$\begin{pmatrix}\langle g|\psi(t)\rangle\\ \langle e|\psi(t)\rangle\end{pmatrix} \qquad (2)$$

When each cosine in Eq. (2) is replaced by one exponential (in magnetic resonance, when each of the two linearly oscillating fields is replaced by a rotating field) we obtain,

$$\frac{d}{dt}\begin{pmatrix}\langle g|\psi(t)\rangle\\ \langle e|\psi(t)\rangle\end{pmatrix}=$$

$$\begin{pmatrix}E_g & b_P\exp(+i\omega_P t)+b_C\exp(+i\omega_C t)\\ b_P^*\exp(-i\omega_P t)+b_C^*\exp(-i\omega_C t) & E_e\end{pmatrix}\times$$

$$\begin{pmatrix}\langle g|\psi(t)\rangle\\ \langle e|\psi(t)\rangle\end{pmatrix}. \qquad (3)$$

This is the starting equation normally adapted for the problem of a two-level system interacting with two classical monochromatic fields having frequencies ω_P and ω_C very close to the qubit's transition frequency, ω_{ge}. The replacement of Eq. (2) by Eq. (3) is called the *generalized rotating-wave approximation* (GRWA). In the GRWA limits, i.e. when $|\omega_{ge}-\omega_P|\ll\omega_{ge}$ and $|\omega_{ge}-\omega_C|\ll\omega_{ge}$, the perturbation approach can be employed if the coupling strengths of the system with the fields are extremely small (since we know that the frequencies of the fields are extremely close to the resonance frequency). As we are pursuing in this work, the inclusion of both counter-rotating components of the two linear fields, i.e. Eq. (2), not only accounts for various processes, besides GRWA allowed transitions, but also provides the correct prediction on various nonlinear features, e.g. the resonance shift, the resonance line-width, et al., of the resonance transition. The importance of the anti-rotating factors become more pronounced when the detuning of the fields, $|\omega_{ge} - \omega_P|$ and $|\omega_{ge} - \omega_C|$ are large, and, therefore, cannot be ignored in the calculations.

The potential energy of transmon qubit has inversion symmetry (parity) but not rotational symmetry [50, 51]. Hence, angular momentum is not conserved (unlike hydrogen atoms). The eigenstates of transmon qubits have definitive parity which determines allowed dipole transitions (only between states with different parities). In general, since the potential energy for superconducting qubits can be tuned, the inversion symmetry for these artificial atoms can be broken and the parity restriction is lifted [48, 50, 51]. Therefore, the two adjacent energy levels can be coupled by even number of photons, and the even valued multiphoton processes can also be observed. The existence of the longitudinal coupling between superconducting qubits and applied magnetic fields has been shown theoretically [52], when the inversion symmetry of the potential energy of the superconducting qubit is broken. When a superconducting qubit is driven by a strong ac field, the time dependent Hamiltonian, which describes the longitudinal coupling (without considering dissipation) is given by,

$$H_L(t) = -\frac{1}{2}[\Delta\sigma_x + \varepsilon_z(t)\sigma_z]. \tag{4}$$

where $\varepsilon_z(t) = \varepsilon_0 + 2b'_P cos(\omega'_P t + \phi_P) + 2b'_C cos(\omega'_C t + \phi_C)$. Here, the parameter $\Delta = 6.25 \times 10^{-3}$ a.u. is called the tunnel splitting and ε_0 is the detuning energy. The amplitudes of the probe and coupler fields are $b'_P = b'_C = 1.125 \times 10^{-1}$ a.u. This is parameterized in the energy unit and is proportional to the ac flux bias [53]. For simplicity we assume $\phi_P = \phi_C = 0$ because they produce no observable effect on the absorption spectra of the qubit.

One should note that the longitudinal coupling, when the unperturbed Hamiltonian has only off-diagonal matrix elements, is equivalent to the transverse coupling when the unperturbed Hamiltonian has only diagonal matrix elements (they both produce the same time evolution). In that case, the Hamiltonian for longitudinal qubit-field coupling, Eq. (4), can be obtained from the transverse form, Eq. (1), if a unitary transformation is applied,

$$H_L(t) = U^{-1} H_T(t) U \quad , \; U = \frac{1}{\sqrt{2}} \begin{pmatrix} 1 & -1 \\ 1 & 1 \end{pmatrix}. \tag{5}$$

The situation, however, is different if the interaction Hamiltonian $H(t)$ contains both the longitudinal and transverse terms, *i.e.*, $H(t) = b(t)\sigma_z + c(t)\sigma_x$. As is the case for the Transmon quibt [50, 51], such system cannot be transformed into a model with only longitudinal or only transverse coupling. Thus, both coupling schemes must be considered.

Recently, we have proposed [32] a graph-theoretical formalism to study generic circuit quantum electrodynamics systems consisting of a two-level qubit coupled with a single-mode resonator in arbitrary coupling strength regimes beyond the rotating-wave approximation. Here, we extend the method to investigate the dynamics of the two-level superconducting artificial atoms driven by two microwave fields. The two above mentioned interacting designs, *i.e.* Eqs. (1) and (4), are modeled by different graph products on colored-weighted graphs which represent the quantum system and the two discrete driving microwave fields.

Fig. (3) schematically illustrates the generation of dressed quasienergy levels as different schemes of graph products between a complete graph, K_2, representing the two-level system, and the probe and coupler fields, represented by two subsequent path graphs of P_∞^P and P_∞^C, respectively. To illustrate the Fourier components of such discretized oscillating external fields, the vertices of the path graphs are assigned with the weights of $n\hbar\omega$, where $n = 0, \pm 1, \pm 2, \pm 3, ...$ (please see the supplemental material A for more details).

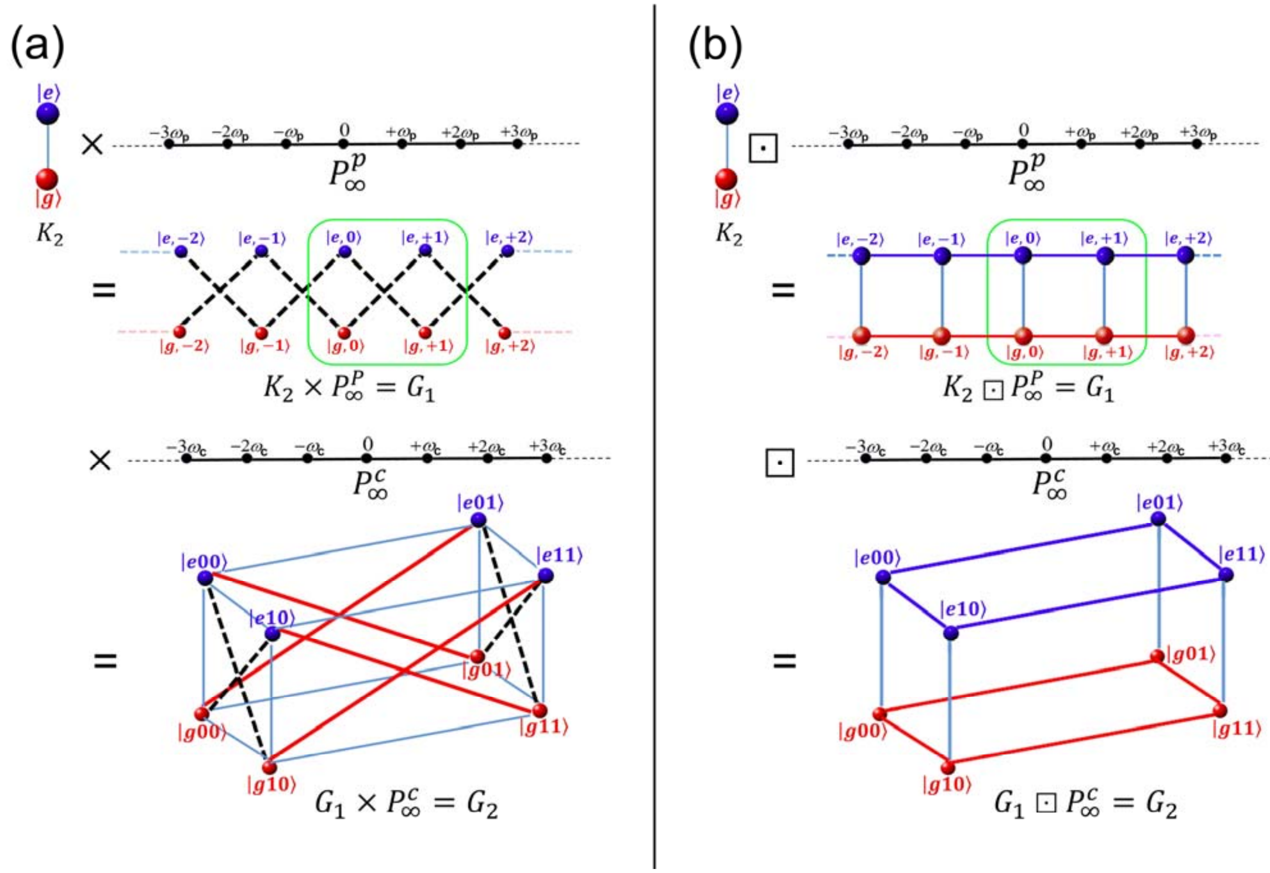

FIG. 3. (Color online) Illustration of (a) transverse, and (b) longitudinal couplings of a two level system, represented by K_2 complete graph, with the probe, represented by P_∞^P path graph, and coupler, represented by P_∞^C path graph, external fields. The direct product, (a), and the Cartesian product, (b) are presented, as schematic exhibition of subsequent interactions of the two-level system with the bichromatic external field. For clarity, the second production is shown only onto the small part of the first product graph, inside the green box. The lighter blue rectangle box in the final product in (a) is to make the pattern easier to follow, and it is not representing any real edges.

After solving the eigenvalue problem for the colored weighted adjacency matrices of the direct and Cartesian products, the time-averaged transition probability between $|g\rangle$ and $|e\rangle$ can be calculated as the probability to go from a single initial vertex on the product graph to a final vertex, summed over all the paths containing the intermediate vertices in the product graph. This can be numerically calculated as [49,46].

$$\bar{P}_{g\to e} = \sum_{n_1 n_2} \sum_{\gamma j_1 j_2} \left| \langle e, n_1 n_2 | a_{\gamma j_1 j_2} \rangle \langle a_{\gamma j_1 j_2} | g, 00 \rangle \right|^2 . \quad (6)$$

Where n_1, n_2 (and also j_1, j_2) are the Fourier index that runs over all the integers. $\gamma = g, e$ are the system indices. The dressed states in the Floquet Hilbert space are $|\gamma, n_1, n_2\rangle = |\gamma\rangle \otimes |n_1\rangle \otimes |n_2\rangle$.The quasienergy eigenvalues of the product adjacency matrix are $a_{\gamma j_1 j_2} = a_{\gamma 00} + j_1 \omega_P + j_2 \omega_C$. The corresponding normalized eigenvectors are $\left| a_{\gamma j_1 j_2} \right\rangle$. Assuming the initial state of the system at time t_0 is $|g\rangle$, Eq. (6) would be representing the transition probability averaged over $(t - t_0)$ and will be always less than or equal to $\frac{1}{2}$. This is associated with the probability of finding the excited state of the qubit in the experiment.

Results and Discussion

The experimental and theoretical transition probabilities are presented, when a transmon superconducting qubit is subject to two near-resonance to resonance microwave fields.

Figs. 4(a, b) correspond to the case when single photon transition condition is satisfied. The dynamics of such process is modeled by the Hamiltonian given in Eq. (1). This system, therefore, can be illustrated by the direct graph product, $K_2 \times P_\infty^P \times P_\infty^C$, as shown in Fig.3(a). As can be seen in this figure, under a monochromatic field, the direct product, $K_2 \times P_\infty^P$, only allows odd-walks transitions in the graph between the single-dressed states. This resembles the population transfer in a Hilbert space splitting in two unconnected subspaces or parity chains, $P = +1, -1$ [45]. The mechanism for the appearance of multiple near-resonance peaks, as can be seen in Figs. 4(a, b), will be revealed by examining the role of the coupler tone in connecting the single-dressed manifolds when the doubly-dressed states form as the vertices of the new direct product graph, $K_2 \times P_\infty^P \times P_\infty^C$. For computational simplicity, the probe frequency is scanned at the adjacency of $\omega_P = 1.0\ \mathrm{a.u.}$ while the two states of the qubit are also separated by $\omega_{ge} = 1.0\ \mathrm{a.u.}$ The main wide vertical and horizontal absorption lines in both the calculated and measured spectra indicate the single photon transition due to the probe and coupler tones, respectively. As a supplemental material B, we attach a video of our calculations showing the time evolution of this plot, Fig. 4(b), when the intensity of the coupler microwave is gradually increased. At this point, it is instructive to look at this result from the intuitive perspective of GRWA. One understands that the time-independent Schrödinger equation of a two-level system in the presence of a single rotating field is equivalent to a 2×2 time-independent Floquet eigenvalue problem with the 2×2 Floquet Hamiltonian [5],

$$H_F^{(2\times2)} = \begin{pmatrix} -0.5\omega_{ge} & b_P \\ b_P^* & 0.5\omega_{ge} - \omega_P \end{pmatrix}. \tag{7}$$

Therefore only one photon can be absorbed or emitted at a time. By introducing a second field (rotating in the same direction as the first one) these 2×2 single-field Floquet Hamiltonians are coupled to one another via the second field in such way that the multiphoton process under investigation can take place only by absorbing (emitting) a photon of the one field, then emitting (absorbing) a photon of the other.

Figs. 4(c, d) present the experimental and theoretical results for the observation of the two-photon transitions. In this case the system is described by the longitudinal coupling Hamiltonian, Eq. (4). As illustrated in Fig. 4(b), the time-independent Floquet matrix for such system can, therefore, be modeled by the subsequent Cartesian products of the two-level system by the probe and coupler microwave fields, $K_2 \square P_\infty^P \square P_\infty^C$. As shown in Fig. 4(c, d), the population transfer can occur by two-photon absorption from a single field (vertical and horizontal absorption lines), or from two different fields (diagonal absorption line). Again, for computational simplicity, the probe frequency is scanned at the adjacency of $\omega_P = 0.5\ a.u.$ while the two states of the qubit are separated by $\omega_{ge} = 1.0$ a.u. Later, we will investigate the underlying mechanism of the fine structure of the fringes at the middle of these plots by scanning ω_P and ω_C along the dashed-green line in Fig. 4(d).

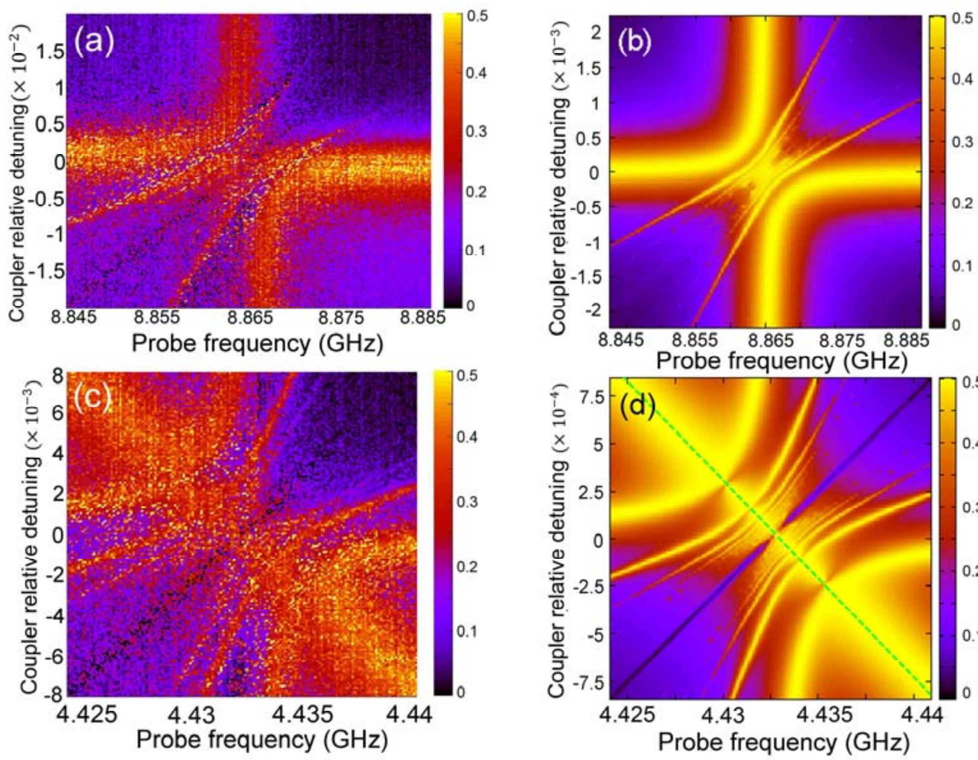

FIG. 4. (Color online) (a) Experimental measurement of the single-photon transitions in a transmon superconducting qubit. (b) Two-mode Floquet result of the transverse coupling of a two-level system with the bichromatic external field. (c) Experimental measurement of the double-photon transitions in a transmon superconducting qubit. (d) Two-mode Floquet result of the longitudinal coupling of a two-level system with the bichromatic external field. The dynamics of the system along the diagonal dashed-green line, will be analyzed later to reveal the mechanism for the central fine pattern. The smaller transition probability of experimental spectra is due to dissipation which was not taken into account in our theoretical calculation.

Fig. 5(a) provides a schematic representation of the doubly-dressed states to explain the appearance of the swallowtail butterfly like patterns in the transition probability contour plots presented in Fig.4. This figure shows the splitting of the energy levels due to multi-photon coupling between the singly-dressed states. The quasienergies and transition probability along the diagonal dashed-green line is given in Fig. 5(b) and Fig. 5(c), respectively. In this case, the transition probability spectrum consists of a symmetric series of dispersion-like sidebands. These sub-harmonic resonances occur when the detuning of the second field is an integer fraction of the Rabi frequency of the resonant field. In other words, the second field is resonant with a *n*-photon interaction between the single dressed states [9]. These resonances are illustrated by the green edges in Fig. 5(a). On each edge, the numeric label indicates the number of photons required to make the resonance between the two states to take place. The avoided crossings in Fig. 5(c) at the position of these sub-harmonic peaks indicate that the lower and upper eigenstates are strongly connected, and that the resonance transitions are well pronounced between the states of the two-level system.

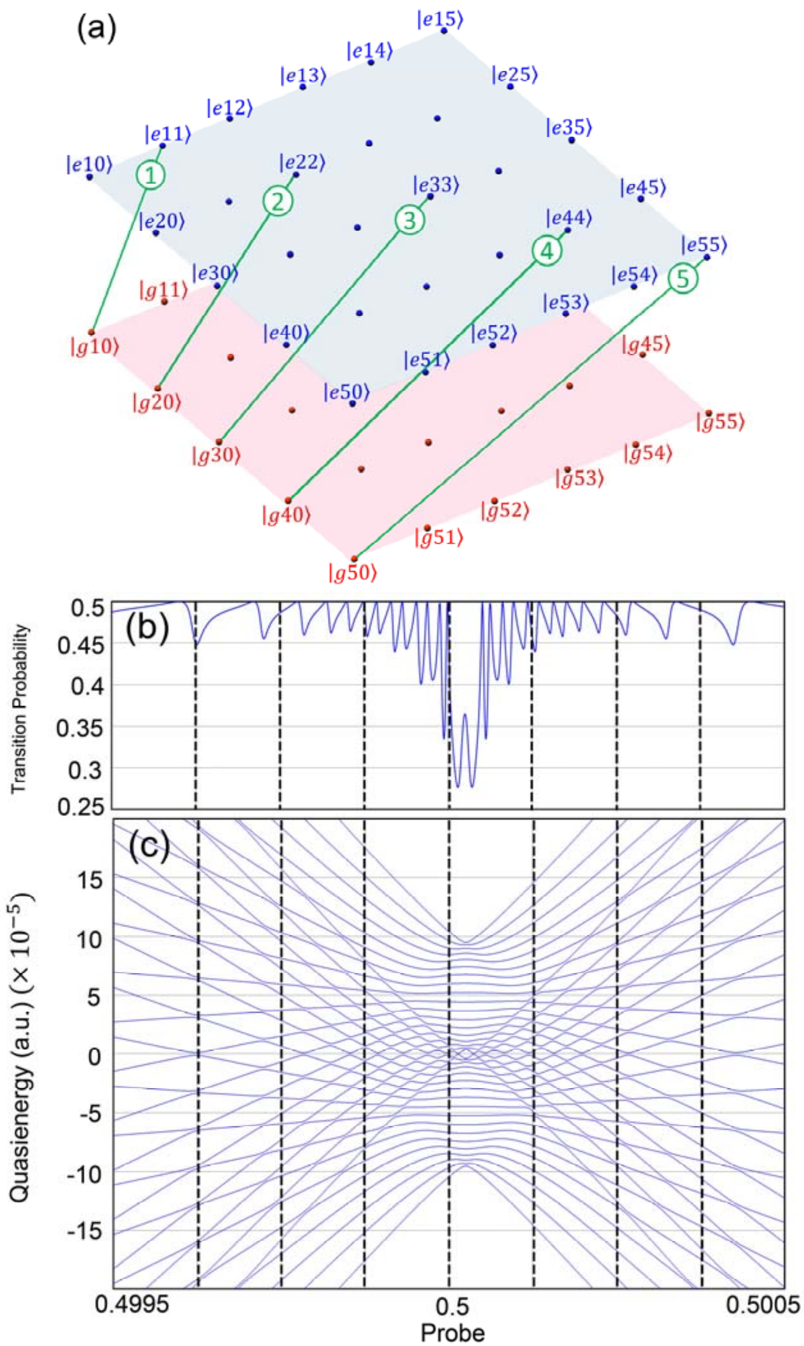

FIG. 5. (Color online) (a) Schematic illustration of the doubly-dressed two-level system. The multiphoton resonances, due to the coupler tone, between the single-dressed states are shown by green edges. The numeric label on each edge indicates the required number of photons to make that resonance happen. (b) The quasienergies, and (c) transition probabilities along with the

dashed-green line in Fig. 4(d). This result corresponds to the case of a superconducting qubit with longitudinal coupling to bichromatic microwave field.

Summary

In summary, we report experimental observation of two distinct quantum interference patterns in the absorption spectra when a transmon superconducting qubit is subject to a bichromatic microwave field. We propose a graph-theoretical representation to model the interaction Hamiltonian. The generalized graph-theoretical method provides a clear physical picture of and gains insight into this intrigue phenomenon. We showed that while the observed absorption spectrum near the single photon resonance can be produced by transverse and/or longitudinal coupling between a two-level system and a bichromatic field the observed absorption spectrum near the two-photon resonance can only be produced by a longitudinal coupling between the qubit and the bichromatic microwave field. These coupling schemes can be modeled by different graph products on colored-weighted graphs. In each case, the intuitive picture provided by the doubly dressed states is used to explain the mechanism and to demonstrate the characteristic features of each case of study. The good agreement between the numerical simulation and experimental data confirms the validity of the proposed graph-theoretical approach. These observations and interpretation may be used not only to generate multi-level tunable energy structures, but also to explore non-classical microwave photons, which are the fundamental elements in the quantum information processing especially in the microwave quantum photonics.

Acknowledgments

S. H. is supported in part by NSF (PHY-1314861). This work was partially supported by the NKRDP of China (Grant No. 2016YFA0301801), NSFC (11474154), PAPD and Dengfeng Project B of Nanjing University. S.I.C. acknowledges the partial support from the Chemical Sciences, Geosciences, and Biosciences Division of the Office of Basic Energy Sciences, U.S. Department of Energy (Grant No. DE-FG02-04ER15504). D.A.T. acknowledges the partial support from Russian Foundation for Basic Research (Grant No. 16-02-00233).

References

[1] S. Richer, and D. DiVincenzo, Phys. Rev. B **93**, 134501 (2016).

[2] P. M. Billangeon, J. S. Tsai, and Y. Nakamura, Phys. Rev. B **91**, 094517 (2015).

[3] S. I. Chu, and D. A. Telnov, Phys. Rep. **390**, 1 (2004).

[4] P. K. Aravind, and J. O. Hirschfelder, J. Chem. Phys. **88**, 4788 (1984).

[5] J. H. Shirley, Phys. Rev. **138**, B979 (1965).

[6] W. D. Oliver, Y. Yu, J. C. Lee, K. K. Berggren, L. S. Levitov, T. P. Orlando, Science **310**, 1653 (2005).

[7] Y. Nakamura, Y. A. Pashkin, and J. S. Tsai, Phys. Rev. Lett. **87**, 246601 (2001).

[8] S. K. Son, S. Han, and S. I. Chu, Phys. Rev. A **79**, 032301 (2009).

[9] A. D. Greentree, C. Wei, S. A. Holmstrom, J. P. D. Martin, N. B. Manson, K. R. Catchpole, and C. Savage, J. Opt. B: Quantum Semiclass. Opt. **1**, 240 (1999).

[10] T. G. Rudolph, H. S. Freedhoff, and Z. Ficek, Opt. Commun. **147**, 78 (1998).

[11] Z. Ficek, and H. S. Freedhoff, Phys. Rev. A **53**, 4275 (1996).

[12] M. Jakob, and G. Y. Kryuchkyan, Phys. Rev. A **57**, 1355 (1998).

[13] C. C. Yu, J. R. Bochinski, T. M. V. Kordich, T. W. Mossberg, and Z. Ficek, Phys. Rev. A **56**, R4381 (1997).

[14] Y. Zhu, Q. Wu, A. Lezama, D. J. Gauthier, and T. W. Mossberg, Phys. Rev. A **41**, 6574 (1996).

[15] S. Papademetriou, M. F. Van Leeuwen, and C. R. Jr. Stroud, Phys. Rev. A **53**, 997 (1996).

[16] F. Forster, M. Mühlbacher, R. Blattmann, D. Schuh, W. Wegscheider, S. Ludwig, and S. Kohler , Phys. Rev. B **92**, 245422 (2015).

[17] A. P. Saiko, R. Fedaruk, A. Kolasa, and S. A. Markevich, Phys. Scr. **85**, 045301 (2012).

[18] A. P. Saiko, R. Fedaruk, and A. Kolasa, J. Phys. B: At. Mol. Opt. Phys. **45**, 235501 (2012).

[19] J. Benhelm, G. Kirchmair, C. F. Roos, Nat. Phys. **4**, 463 (2008).

[20] S. Y. Zhu, and M. O. Scully, Phys. Rev. Lett. **76**, 388 (1996).

[21] Z. Ficek, and T. Rudolph, Phys. Rev. A **60**, R4245 (1999).

[22] Y. He, Y. M. He, J. Liu, Y. J. Wei, H.□Y. Ramírez, M. Atatüre, C. Schneider, M. Kamp, S. Höfling, C. Y. Lu, and J. W. Pan, Phys. Rev. Lett. **114**, 097402 (2015).

[23] M. Peiris, K. Konthasinghe, Y. Yu, Z. C. Niu, and A. Muller, Phys. Rev. B **89**, 155305 (2014).

[24] C. C. Tannoudji, and S. Haroche, J. Phys. France **30**, 153 (1969).

[25] S. Haroche, Rev. Mod. Phys. **85**, 1083 (2013).

[26] S. I. Chu, and W. P. Reinhardt, Phys. Rev. Lett. **39**, 1195 (1977).

[27] G. Oelsner, P. Macha, O. V. Astafiev, E. Il'ichev, M. Grajcar, U. Hübner, B. I. Ivanov, P. Neilinger, and H. G. Meyer, Phys. Rev. Lett.**110**, 053602 (2013).

[28] J. Q. You, and F. Nori, Nature **474**, 589 (2011).

[29] Y. S. Greenberg, Phys. Rev. B **76**, 104520 (2007).

[30] C. M. Wilson, T. Duty, F. Persson, M. Sandberg, G. Johansson, and P. Delsing, Phys. Rev. Lett. **98**, 257003 (2007).

[31] J. M. Fink, R. Bianchetti, M. Baur, M. Göppl, L. Steffen, S. Filipp, P. J. Leek, A. Blais, and A. Wallraff, Phys. Rev. Lett. **103**, 083601 (2009).

[32] H. Z. Jooya, K. Reihani, and S. I. Chu, Sci. Rep. **6**, 37544 (2016).

[33] H. C. Sun, Y. X. Liu, H. Ian, J. Q. You, E. Il'ichev, and F. Nori, Phys. Rev. A **89**, 063822 (2014).

[34] J. Clarke, and F. K. Wilhelm, Nature (London) **453**, 1031 (2008).

[35] Z. L. Xiang, S. Ashhab, J. Q. You, and F. Nori, Rev. Mod. Phys. **85**, 623 (2013).

[36] I. Buluta, S. Ashhab, and F. Nori, Rep. Prog. Phys. **74**, 104401(2011).

[37] S. E. Harris, J. E. Field, and A. Imamoglu, Phys. Rev. Lett. **64**, 1107 (1990).

[38] M. Fleischhauer, A. Imamoglu, and J. P. Marangos, Rev. Mod. Phys. **77**, 633 (2005).

[39] S. H. Autler, and C. H. Townes, Phys. Rev. **100**, 703 (1955).

[40] M. A. Sillanpää, J. Li, K. Cicak, F. Altomare, J. I. Park, R. W. Simmonds, G. S. Paraoanu, and P. J. Hakonen, Phys. Rev. Lett. **103**, 193601 (2009).

[41] S. Novikov, J. E. Robinson, Z. K. Keane, B. Suri, F. C. Wellstood, and B. S. Palmer, Phys. Rev. B **88**, 060503(R) (2013).

[42] J. Li, G. S. Paraoanu, K. Cicak, F. Altomare, J. I. Park, R. W. Simmonds, M. A. Sillanpää, and P. J. Hakonen, Sci. Rep. **2**, 645(2012).

[43] I. C. Hoi, C. M. Wilson, G. Johansson, J. Lindkvist, B. Peropadre, T. Palomaki, and P. Delsing, New J. Phys. **15**, 025011(2013).

[44] H. Ian, Y. Z. Liu, and F. Nori, Phys. Rev. A **81**, 063823 (2010).

[45] G. J. Dolan, Appl. Phys. Lett. **31**, 337 (1977).

[46] M. Gong, X. Wen, G. Sun, D. Wei Zhang, D. Lan, Y. Zhou, Y. Fan, Y. Liu, X. Tan, H. Yu, Y. Yu, S. L. Zhu, S. Han, and P. Wu , Sci. Rep. **6**, 22667 (2016).

[47] M. D. Reed, L. DiCarlo, B. R. Johnson, L. Sun, D. I. Schuster, L. Frunzio, and R. J. Schoelkopf, Phys. Rev. Lett. **105**, 173601 (2010).

[48] Y. J. Zhao, Y. L. Liu, Y. X. Liu, and F. Nori, Phys. Rev. A **91**, 053820 (2015).

[49] T. S. Ho, and S. I. Chu, J. Phys. B: At. Mol. Phys. **17**, 2101 (1984).

[50] J. Koch, T. M. Yu, J. Gambetta, A. A. Houck, D. I. Schuster, J. Majer, A. Blais, M. H. Devoret, S. M. Girvin, and R. J. Schoelkopf, Phys. Rev. A **76**, 042319 (2007).

[51] J. A. Schreier, A. A. Houck, J. Koch, D. I. Schuster, B. R. Johnson, J. M. Chow, J. M. Gambetta, J. Majer, L. Frunzio, M. H. Devoret, S. M. Girvin, and R. J. Schoelkopf, Phys. Rev. B 77, 180502(R) (2008).

[52] Y. X. Liu, C. X. Yang, H. C. Sun, and X. B. Wang, New J. Phys. **16**, 015031 (2014).

[53] D. M. Berns, W. D. Oliver, S. O. Valenzuela, A. V. Shytov, K. K. Berggren, L. S. Levitov, and T. P. Orlando, Phys. Rev. Lett. **97**, 150502 (2006).